Earthquake Geotechnical Engineering for Protection and Development of Environment and Constructions – Silvestri & Moraci (Eds)
© 2019 Associazione Geotecnica Italiana, Rome, Italy, ISBN 978-0-367-14328-2

Design of hazard resilient steel pipe using numerical simulations and large scale testing

B.A. Berger
Thornton Tomasetti, San Francisco, CA, USA

B.P. Wham
Center for Infrastructure, Energy, and Space Testing, University of Colorado Boulder, USA

T.D. O'Rourke
Geotechnical Lifelines Group, School of Civil and Environmental Engineering, Cornell University, USA

ABSTRACT: Large diameter steel pipe is a critical component of water transmission infrastructure around the world and carries a significant percentage of consumed water in transmission lines ranging in diameter from 0.6 m (24 in.) to 3.7 m (144 in.). Failure of these large diameter lifelines in areas of high seismicity can prove catastrophic by hindering fire suppression efforts and access to clean drinking water. This paper investigates current design practices for continuously welded steel pipe and addresses the applicability to new hazard-resistant design feature. Full-scale tests were performed at Cornell University's Geotechnical Lifelines Large-Scale Testing Facility to determine the efficacy of an innovative steel pipe for fault crossing (SPF). The pipes were tested at quarter scale with a diameter of 0.22 m (8.5 in.). High fidelity three-dimensional finite element models were calibrated by large-scale test results and used to predict the response of a 0.86 m (34 in.) diameter pipeline.

1 INTRODUCTION

Large diameter steel pipelines are a critical component of water transmission infrastructure. Failure of these lifelines due to large earthquake-induced ground deformations would have catastrophic effects on emergency response, including fire suppression efforts, and sever access to clean water for millions of people. Earthquake-induced ground deformations include fault offset, liquefaction, lateral spreading, and landslides. Other forms of ground displacement such as undermining can be caused by earthquake-induced tsunamis.

Pipelines in areas prone to earthquake-induced liquefaction and other sources of large ground displacement need to accommodate deformation through movement at joints or along the pipe body. In some instances, a pipe can undergo considerable cyclic loading due to the effects of near field velocity pulses.

Steel pipelines are typically constructed using one of two methods: (1) welded lap joints or (2) full penetration circumferential butt welds. Karamanos et al. (2017) provide a rigorous review of current codes and design standards for steel pipelines. Tensile strain limits can range from 1–5% depending on the applicable standard. All standards known to the authors omit exceptions or provisions for local, highly deformable sections that concentrate plastic strain.

This paper focuses on the direct tension and cyclic portions of an experimental program performed at Cornell University's Large-Scale Lifelines Testing Facility for JFE Engineering Corporation's (herein referred to as JFE) wave feature for Steel Pipe Crossing Faults (SPF). The feature is a local, highly deformable section of the pipe designed to accommodate high tensile, compressive, and rotational movements while allowing the pipe barrel to remain in a relatively low strain state. The wave feature also limits cross-sectional area reduction in the

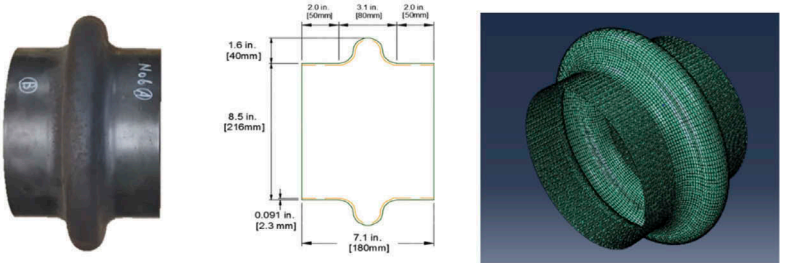

Figure 1. SPF wave feature (a) plan view, (b) dimensions as tested, and (c) finite element discretization.

deformed section. Figure 1 shows the wave feature, its dimensions as tested, and a finite element discretization of the feature covered in this work.

The pipe barrel for all specimens was 216 mm (8.5 in.)-diameter steel pipe with average wall thickness, modulus, and yield strength of 2.3 mm (0.091 mm), 229 GPa (33,200 ksi), and 333MPa (48.3 ksi), respectively. Tensile coupon tests performed on specimens machined from the pipe wall are described by Berger et al. (2017). The SPF is connected to the pipe body via full penetration butt welds.

The wave was characterized by its ability to handle tensile, compressive, cyclic, and rotational forces at ¼ scale. The intended use of such features is for pipelines of ~0.8 m (34 in.) or greater. This scaling will be explored by the finite element model developed herein.

The culmination of testing was a full-scale fault rupture simulation where a 216 mm (8.5 in.) diameter pipeline equipped with wave feature on either side of a right-lateral strike-slip fault accommodated 600 mm (24 in.) of fault movement without a loss of pressure or a significant reduction in cross-sectional area. Wham et al. (2018) presents these findings in detail. Project reports for compression, bending, and fault rupture are provided by Wham et al. (2016) and details of the tension and cyclic tests are available in Berger et al. (2017).

The results of this paper can be used to qualify allowable strain limits from axial and rotational deformations for the design of steel transmission pipelines that incorporate seismic-resistant technology, such as SPF. The paper provides test data that help future standards account for such technologies.

2 AXIAL TENSION AND CYCLIC TESTS ON WAVE FEATURE AND STRAIGHT PIPE

Following experimental procedures designed to characterize the performance of SPF in compression and bending, additional tests were needed to qualify the system for tensile and transient ground motions. Specifically, an experiment was designed to quantify the axial force capacity reduction of the SPF under cyclic loading. A straight pipe tension test was performed without a wave feature to compare its performance with that of the SPF and to calibrate the finite element model discussed later.

Specimens were manufactured via robotic welding to be 3.05 m (120 in.) long with the wave centered at 1.53 m (60 in.) from each end flange weld, as shown in Figure 2. Flanges were circumferentially welded to the pipe ends to accept imposed axial load as well to seal and pressurize the pipe with water.

2.1 *Instrumentation*

The straight pipe specimen, without SPF, was instrumented with four planes of strain gages at 8, 17, 30, and 60 in. (200, 430, 760, and 1500 mm) from the actuator side of the specimen, corresponding to one, two, three and a half, and seven diameters away from the end flange weld (Figure 2a).

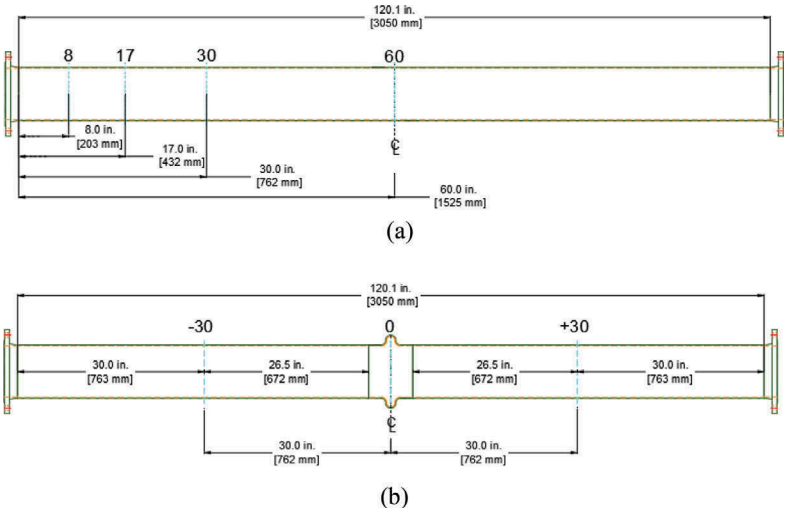

Figure 2. Strain gage layout of (a) straight pipe and (b) pipe with SPF.

The specimens with SPFs were instrumented with 3 planes of strain gages, shown in Figure 2b, and denoted as -30, 0, and 30 for their positions relative to the centerline of the wave. This corresponds to dimensions of -30 in., 0 in., and 30 in. (-762mm, 0 mm, 762mm) respectively.

A total of 20 strain gages were used for each test. Planes -30 and 0 each consisted of four axial and four circumferential gages while plane +30 consisted of four axial gages. At all planes, gages were applied to the crown, invert, and both spring lines of the pipe surface. Additional details of the strain gage measurements for all tests are provided by Berger et al. (2017). During the experiment, the 20 strain channels were monitored continuously in combination with actuator load and displacement, internal pressure, a redundant set of end load cells, and a series of string potentiometers placed across the wave. These string potentiometers, denoted in Figure 3 as "SP Wave Displacements" were critical in understanding the localized behavior of the wave absent influence from the rest of the pipe.

2.2 *Test procedure for direct tension of straight pipe (TTS) and SPF (TTW1)*

After the specimen was instrumented and centered in the load frame, the test sequence was initiated by starting the data acquisition system and laboratory hydraulic systems.

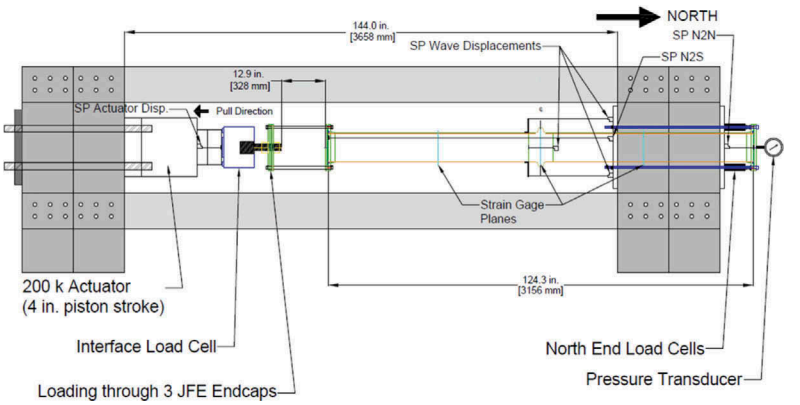

Figure 3. Plan view of axial tension and cyclic test setup.

The data sampling rate was 2 Hz. The north end load cells, mounted on rods, were slowly tightened. They were adjusted to about 4.45 kN (1 kip) each, totaling 17.8 kN (4 kips) of force. No load was transmitted to the specimen since the south end was free to move. Then the nuts on the south end, where the pipe flange connects to the actuator with 19 mm (0.75 in.) high strength threaded rods, were tightened. These adjustments ensured concentric initial loading conditions and restrained the pipe from axial movement due to internal pressure. Approximately 550 kPa (80 psi) of internal water pressure was applied. The measuring systems were checked and an initial actuator displacement of 91 mm (3.6 in.) was applied.

The actuator used for this test has a stroke of 100 mm (4 in.). Following the initial displacement step, the specimen was unloaded and the actuator was extended. The loading rods connecting the actuator to the south end flange were repositioned to apply a second loading increment. Total axial displacements of 112 mm (4.4 in.) and 137 mm (5.4 in.) were applied for the straight pipe (TTS) and SPF direct tension test (TTW1), respectively.

2.3 *Test procedure for cyclic test of SPF (TTW2)*

Initial setup for the second tension test, TTW2, was similar to the previous tests. The north end load cells, mounted on threaded rods, were tightened to about 22.25 kN (5 kips) each, totaling 89 kN (20 kips) of axial force. No force was transmitted to the specimen since the south end was free to move. Since the north load cells can only measure compressive force, preloading provided a means of measuring both applied tensile and compressive axial force during cyclic loading. Next, the nuts were tightened on the south end where the pipe flange and 19 mm (0.75 in.) high strength threaded rods were connected to the actuator. The pipe was filled with water and pressure was maintained between 0 and 69 kPa (0–10 psi) for the entire test. The testing was performed at very low to negligible pressure that provides less resistance to flattening of the SPF wave feature than the 550 kPa (80 psi) used in TTW1. The ±50 mm (2 in.) stroke actuator was positioned at its center of travel, which is identified as 0 displacement. Positive and negative displacements are related to tensile and compressive forces, respectively.

Figure 4a provides the actuator displacement vs. time for the initial cyclic portion of the test sequence. Episodes A through I in the figure identify each applied displacement increment. Displacement Episode B with 0 mm to -40 mm (-1.57 in.) of actuator displacement was applied at a rate of 25 mm (1.0 in.) per minute to impose compressive displacement consistent with SPF deformation capacity. After this step, the actuator was retracted to its initial position of 0 displacement (Episode C). Cyclic motion of ± 30 mm (1.15 in.) was imposed on the specimen, starting with positive displacement at a frequency of 0.017 hz for two cycles (Episodes D through G). Following the two cycles of loading, a subsequent 63 mm (1.57 in.) of tensile displacement was applied to the specimen. This displacement sequence is shown vs. time in Figure 4a. The pipe was then unloaded and disconnected from the actuator. The actuator was fully extended and the end flange was reconnected. A monotonic ramp from -50 mm (-2 in.) to +50 mm (+2 in.) at a rate of 25 mm (1.0 in.) per minute was applied to the specimen. This process of unloading and reloading was repeated after each subsequent pull. The applied load vs. time for the entire test is shown in Figure 4(b).

2.4 *Test results*

TTS accommodated 112 mm (4.4 in.) of axial displacement at a peak force of 600 kN (135 kips) (Figure 5). Failure was characterized by a weld fracture at the north end flange. It reached 1% strain in the pipe body at an actuator displacement of 31.5 mm (1.24 in.). TTW1

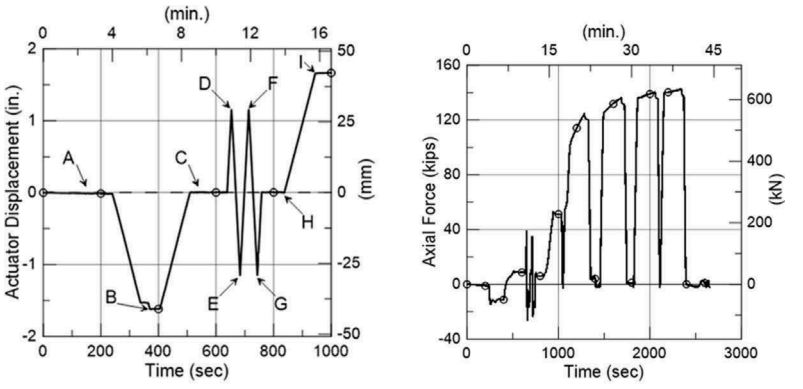

(a) (b)

Figure 4. SPF Cyclic (a) actuator displacement and (b) axial force vs. time.

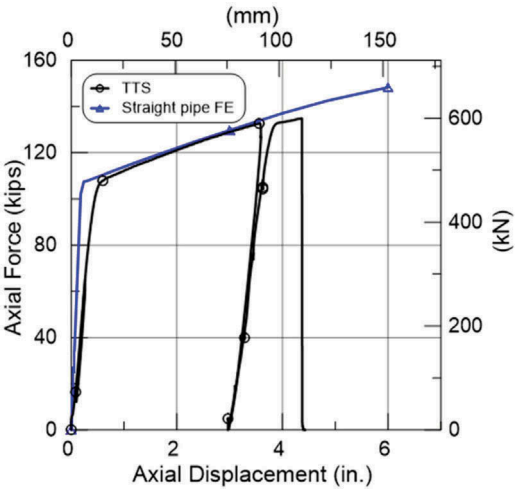

Figure 5. Material calibration using straight pipe tension test.

failed at an actuator displacement of 137 mm (5.4 in) and force of 592 kN (133 kips) caused by a weld fracture at the south flange. This force-displacement relationship is plotted in Figure 6. TTW1 reached 1% strain in the pipe body at an actuator displacement of 76 mm (3 in.). Figure 7 shows the pretest wave feature in its undeformed state followed by successive displacement conditions encountered throughout the testing sequence. As shown in the Figure 7 deformation sequence, the cross-sectional area reduction and accompanying hoop compressive strain that occurs as the wave is pulled in tension causes longitudinal buckling to propagate around the circumference.

The loading steps outlined in the previous section are shown in Figure 8a through i for TTW2. The SPF was able to accommodate 356 mm (14 in.) of actuator displacement and a peak force of 630 kN (142 kips), data shown in Figure 6. The test was stopped because the displacement limit of the loading frame was reached. Through cyclic motions, the strains in the pipe body remained well below elastic limits. It did not reach 1% strain until an actuator displacement of 82.3 mm (3.24 in.)

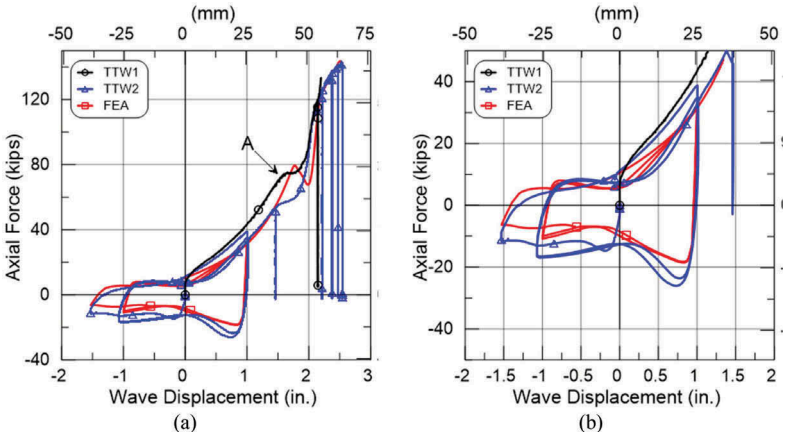

Figure 6. Axial force vs. wave displacement with overlaid FEA for (a) the entire test sequence and (b) magnification of the cyclic displacement stages.

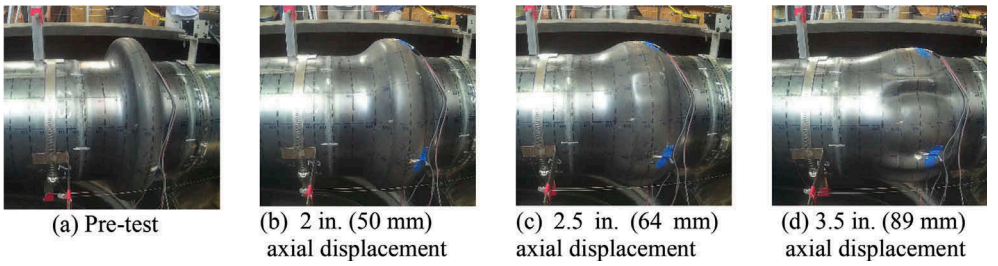

Figure 7. TTW1 SPF deformed shape at various imposed displacements.

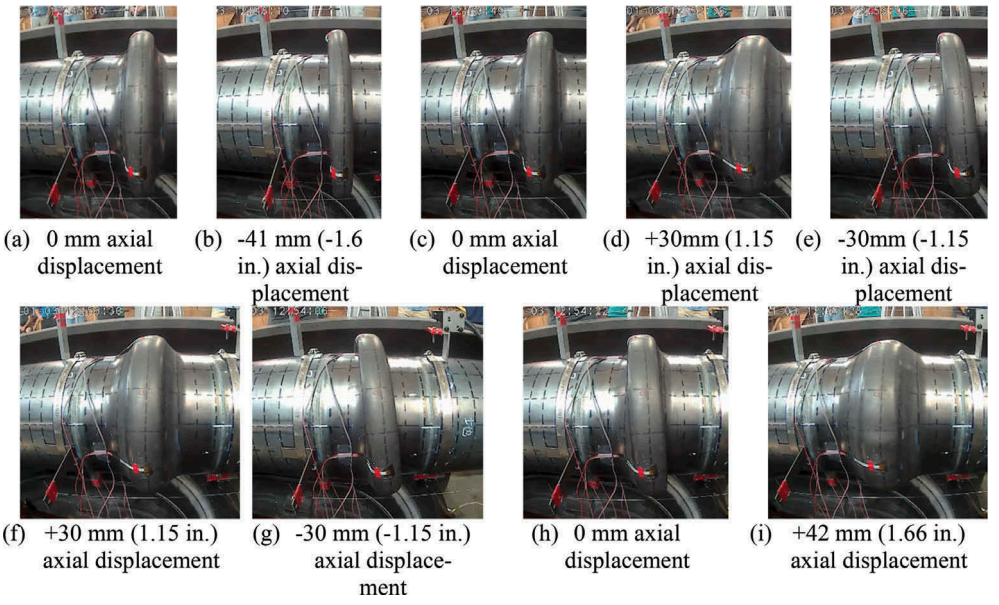

Figure 8. SPF through cyclic motion.

3 FINITE ELEMENT MODELING OF SPF FEATURE

A three-dimensional finite element model of the SPF, shown in Figure 9a, was developed using python scripts to generate the geometry and Abaqus 6.11 (Abaqus 2011) for the analysis. It was necessary to model the entire three-dimensional surface due to nonlinear circumferential buckling of the wall that occurs as the SPF flattens.

A four-node shell element of the S4 family was selected due to the thin walled nature of the pipe. A parametric study of element size was performed to select a size appropriate for representing the curved surface of the wave feature and pipe. Two hundred and fifty elements in the circumferential direction with a longitudinal spacing of 2.54 mm (0.1 in.) were selected to provide computational efficiency and reproducible results. From this study the benefits of the S4Rs, reduced integration shell elements, became clear: computational time decreased and apparent differences in precision were negligible. The S4Rs were used throughout for all three-dimensional models.

As mentioned earlier, the straight pipe tension test results (TTS) were used to calibrate the material properties of the SPF. One dimensional models with beam elements were used to characterize the response. Aside from the residual stress field that is induced in the wave during manufacturing (outside the scope of this study), there are longitudinal and circumferential welds throughout the specimens that affect overall stiffness and performance. It is not possible to capture the effects of these welds in uniaxial tension tests of either plate steel specimens or specimens cut from the pipe wall, as discussed by Wham et al. (2016), Wham et al. (2017), and Berger et al. (2017). Of particular interest is the location of the knee in the force-displacement response, shown in Figure 5, which is indicative of material response beyond the linear-elastic limit. The difference in stiffness between the FEA and TTS graphs is most likely due to seating adjustments in the loading and measurement systems at the start of the large-scale tests. These adjustments did not have a significant effect on pipe and wave feature performance in the nonlinear range of force vs displacement response.

The model shows good agreement with the large-scale test results, with the exception of locating the knee, as shown in Figure 6a, demarcation "A." The modeling provides a slightly conservative estimate of axial force throughout cyclic motions and can serve as a reasonable design tool for implementation of this product, as seen in Figure 6b.

The Bauschinger effect (Rice 1975) was mimicked through kinematic hardening in Abaqus to allow for the movement of the Mises yield surface during cyclic motion. Initially linear kinematic hardening was selected, but due to large plastic strains this was not feasible. Instead a nonlinear kinematic hardening modeling was employed and provided refined estimates of cyclic stresses. A noteworthy deviation of the FEA model from the test results is the location of the knee point, when the wave feature exhibits a nonlinear response due to circumferential buckling to accommodate large tensile deformation. It is the opinion of the authors that this inherent attribute is caused by the hot or cold working of the material during the SPF forming process. The forming process was not disclosed to the authors so a reasonable estimate of the residual stress field caused by temperature or work-hardening is not possible.

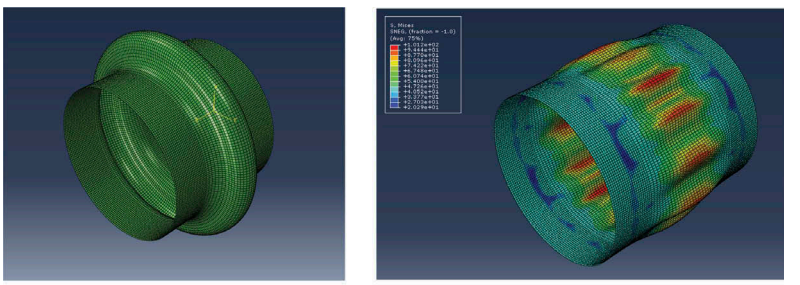

(a) (b)

Figure 9. Three-dimensional finite element model of SPF in (a) undeformed and (b) deformed shape.

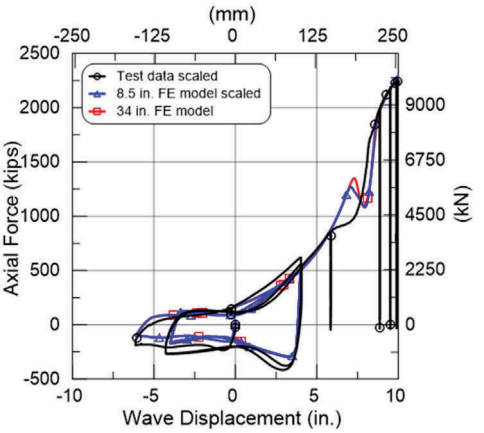

Figure 10. Axial force vs. wave displacement of 1/4 and full-scale models.

3.1 *Scalability*

A new model was developed using python scripts with parameters including thickness, radius, and displacement scaled by a factor of 4 to achieve the intended design size of SPF. To preserve consistent element aspect ratio between models, the number of circumferential nodes was not altered. Instead, the longitudinal spacing was increased from 2.54 mm (0.1 in.) to 10.2 mm (0.4 in.)

Figure 10 shows that the results of both ¼ scale testing and modelling are scalable. The axial forces from the cyclic experiment and model were multiplied by a factor of 4^2 to account for the increase in pipe cross-sectional area, denoted as "test data" and "8.5 in. FE model" scaled, respectively. The experimental and modeled displacements were increased by a factor of 4. The resulting analogs are nearly identical to the results of the full-scale numerical model (denoted as "34 in. FE model").

4 CONCLUSIONS

A series of large-scale tests were performed on a 216 mm (8.5 in.) diameter steel pipe at Cornell University's Large-Scale Lifelines Testing Facility. The results of this experimental program provided input to investigate the efficacy of the finite element method in scalable modelling of complex geometries and large plastic deformation.

Finite element models show that the ¼ scale testing and numerical model results provide a suitable basis for predicting the performance of a 0.86 m (34 in.) diameter pipe with a wave feature from the simulation of a 0.22 m (8.5 in.) counterpart. Future design can therefore take advantage of scalable testing in which plastic strains are confined locally in special features that accommodate large axial deformation. Code updates will need to be substantiated by finite element modelling corroborated by full or partial scale testing.

Assuming the most stringent tensile deformation limits reported by Karamanos et al. (2017), the SPF will reach a strain limit of 1% within 12.75 mm (0.5 in.) of axial movement. Testing has shown that the high plastic strain in the wave allows the strain in the pipe body to remain low, but reach global strains of over 2.5% before the tensile strain in the pipe barrel reaches a limit of 1%. Although developed finite element models omitted the pipe body, it would be relatively straightforward to incorporate beam elements tied to the SPF to assess pipe barrel strains. With the high degree of accuracy to which the SPF was modelled, it is reasonable to assume that the pipe strains would compare well with test results.

Pipeline response to earthquake-induced ground deformation must accommodate combinations of axial and rotational movement. This paper focused specifically on the SPF's ability

to withstand tensile and compressive movements at deformation levels consistent with upper bound near field velocity pulses as well as substantial permanent tensile deformation.

Future numerical investigation is recommended to investigate large bending deformations which will allow for the development of three-dimensional fault rupture models to explore parametrically how the SPF can perform in a single configuration with multiple fault crossing angles.

ACKNOWLEDGEMENTS

The authors would like to thank Addie Lederman, Andrew Shakalis, Margaret Stack, and Dr. Chalermpat Pariya-Ekkasut, who contributed greatly to this project. Significant gratitude is extended to our beloved lab manager, Tim Bond, for his unrelenting work and dedication. Thanks is extended to JFE Engineering Corporation for funding this research.

REFERENCES

ABAQUS, Inc., (2011), ABAQUS Standard, Providence, RI.

Berger, B.A., Wham, B.P., O'Rourke, T.D., Stewart, H. (2018). Direct Tension and Cyclic Testing of JFE SPF Wave Feature, Ithaca, NY: Cornell University.

Karamanos, S.A., Sarvanis, G.C., Keil, B., & Card, R.J. (2017). "Analysis and Design of Buried Steel Water Pipelines in Seismic Areas". *Journal of Pipeline Systems Engineering and Practice*, *8*(4), 4017018. doi.org/10.1061/(ASCE)PS.1949-1204.0000280

Rice, J. R., "Continuum Mechanics and Thermodynamics of Plasticity in Relation to Microscale Deformation Mechanisms," Constitutive Equations in Plasticity, Argon, A. S. Editor, MIT Press, Cambridge, Massachusetts, 1975

Wham, B.P., Berger, B.A., & O'Rourke, T.D. (2019) "Hazard-resistant Steel Pipeline Response to Large Fault Rupture." *Proceedings, Geo-Congress 2019*, Philadelphia, Pennsylvania, March 24–27. *(accepted)*

Wham, B.P., Berger, B.A., Pariya-Ekkasut, C., O'Rourke, T.D., Stewart, H.E., Bond, T.K. (2018) "Achieving Resilient Water Networks: Experimental Performance Evaluation." *Proceedings, 11th U.S. National Conference on Earthquake Engineering*, Los Angeles, California, June 25–29.

Wham, B.P., O'Rourke, T.D., Stewart, H.E., Bond, T.K., & Pariya-Ekkasut, C. (2016). Large-Scale Testing of JFE Steel Pipe Crossing Faults: Testing of SPF Wave Feature to Resist Fault Rupture. Ithaca, NY: Cornell University.

Wham, B.P., Pariya-Ekkasut, C., Argyrou, C., Stack, M., O'Rourke, T.D., Stewart, H.E., Nakazono, H., Hasegawa, N. (2017) "Large Axial Deformation Performance of Steel Pipeline Designed for Fault Crossings." *Proceedings, ASCE Pipelines Conference, Phoenix, Arizona*, Aug. 6–9, Paper ID: 118.